Med Chem Res (2014) 23:2252–2263
DOI 10.1007/s00044-013-0820-0

MEDICINAL CHEMISTRY RESEARCH

ORIGINAL RESEARCH

Molecular docking and 3D-QSAR studies on the MAPKAP-K2 inhibitors

Eslam Pourbasheer · Roya Bazl · Massoud Amanlou

Received: 2 July 2013 / Accepted: 1 October 2013 / Published online: 15 October 2013

Abstract Mitogen-activated protein kinase-activated protein kinase 2 (MAPKAP-K2) has been identified as a drug target for the treatment of inflammatory diseases. Therefore, there is an urgent need to develop new classes of MAPKAP-K2 inhibitors. To understand the structure activity correlation of MAPKAP-K2 inhibitors, we have carried out a molecular docking study and three-dimensional quantitative structure–activity relationship (3D-QSAR) modeling. Both comparative molecular field analysis ($r^2_{cv} = 0.602$, $r^2_{ncv} = 0.955$) and comparative molecular similarity indices analysis ($r^2_{cv} = 0.546$, $r^2_{ncv} = 0.891$) models were generated using the training set on the basis of the common substructure-based alignment and gave reasonable results. The structural insights obtained from both the 3D-QSAR contour maps and molecular docking help to better interpret the structure activity relationship. The results obtained from this study will be useful in the design of potent MAPKAP-K2 inhibitors.

Keywords Molecular docking 3D-QSAR · CoMFA · CoMSIA · MAPKAP-K2 inhibitors

Introduction

Tumor necrosis factor-α (TNF-α) is implicated in several inflammatory diseases such as rheumatoid arthritis, psoriasis, multiple sclerosis, inflammatory bowel disease, endotoxic shock, osteoporosis, Alzheimer's disease and also in congestive heart failure (Camussi and Lupia, 1998; Dinarello, 1991; Arend and Dayer, 1990; Dayer and Demczuk, 1984). Mitogen-activated protein kinase-activated protein kinase-2 (MAPKAP-K2) is an intracellular substrate of p38 which is a member of Ser-Thr protein kinase superfamily that also includes c-Jun N terminal kinase (Cobb and Goldsmith, 1995; Gille *et al*., 1992). MAPKAP-K2 is regulated through direct phosphorylation by MAP Kinase, and regulates cytokine production via a post-transcriptional mechanism (Kotlyarov *et al*., 1999; Winzen *et al*., 1999). The p38 mitogen-activated protein (MAP) kinase pathway has been shown to play an important role in the production of TNF-α and other cytokines (Adams *et al*., 2001; Lee *et al*., 1994). This pathway has, therefore, been of particular interest for the discovery of new anti-inflammatory agents. Several groups have subsequently reported programs also designed to develop anti-inflammatory therapies through the generation of inhibitors of MAPKAP-K2 (Anderson *et al*., 2007; Goldberg *et al*., 2008; Schlapbach and Huppertz, 2009; Trujillo *et al*., 2007; Xiong *et al*., 2008). Recently, pyrazolo[1,5-α] pyrimidine derivative has been reported to be selective inhibitors for mitogen-activated protein kinase-activated protein kinase-2 (Kosugi *et al*., 2012).

A successful three-dimensional quantitative structure–activity relationship (3D-QSAR) model not only helps in better understanding of the structure–activity relationship of any class of compounds but also ensures the researcher an in-depth analysis of the lead compounds in the further studies. Comparative molecular field analysis (CoMFA) (Cramer *et al*., 1988) and comparative molecular similarity indices analysis (CoMSIA) (Klebe *et al*., 1994) are two 3D-QSAR methods that have been successfully employed in

E. Pourbasheer
Young Researchers and Elite Club, Ardabil Branch, Islamic Azad University, Ardabil, Iran

R. Bazl · M. Amanlou (✉)
Department of Medicinal Chemistry, Drug Design and Development Research Center, Faculty of Pharmacy, Tehran University of Medical Sciences, Tehran, Iran
e-mail: amanlou@tums.ac.ir

drug design. In CoMFA, the biologic activity of molecules is correlated with their steric and electrostatic interaction energies. In CoMSIA, similarity indices are calculated at regularly placed grid points for the aligned molecules. CoMSIA includes additional molecular descriptors such as hydrophobic fields and hydrogen bond donor and acceptor fields.

In this work, molecular modeling studies of the MAPKAP-K2 inhibitors were performed using 3D-QSAR and docking approach. We have used CoMFA and CoMSIA methodologies to understand the influence of different physicochemical and structural parameters on MAPKAP-K2 inhibitors (Kosugi *et al*., 2012). However, as an efficient approach for investigating protein–ligand interactions, molecular docking plays a key role in rational drug design (Drews, 2000). So, protein–ligand interactions were investigated using docking in the present paper. The reliability and robustness of the developed best 3D-QSAR models were estimated by the bootstrapping analysis, ten-fold cross-validation and *Y* randomization test. In the current study, we are presenting, for the first time, a computational study on the series of pyrazolo[1,5-α] pyrimidine derivative compounds. The developed models could provide some helpful clues in the future synthesis of highly potent MAPKAP-K2 inhibitors.

Materials and methods

Data sets and alignment

Series of pyrazolo[1,5-α] pyrimidine derivatives as potent MAPKAP-K2 inhibitors reported by Kosugi et al., were chosen in this study (Kosugi *et al*., 2012). In the total set of the 36 compounds reported, 29 compounds were used as a training set, and the remaining 7 compounds were used as a test set, based on a random selection. The inhibition activity data [IC_{50} (μM)] for pyrazolo[1,5-α] pyrimidine derivatives was converted to the negative logarithmic scale pIC_{50} [−log IC_{50} (M)] and then used as dependent variables in the CoMFA and CoMSIA calculations. The test set compounds were selected by considering both the distribution of biological data and structural diversity. The chemical structures and corresponding pIC_{50} values for studied compounds for both the training and test sets are presented in Table 1. It can be seen that except the highest and lowest activity compounds were included in the training set, and the test set compounds have a range of biologic activity values similar to that of the training set.

The 3D structures of the studied compounds were constructed using the standard tools available in the SYBYL package. Energy minimization was performed using the Tripos force field (Clark *et al*., 1989) with a distance-dependent dielectric and the Powell conjugate gradient algorithm with a convergence criterion of 0.01 kcal/mol Å. Partial atomic charges were calculated using the Gasteiger-Hückel method (Gasteiger and Marsili, 1980).

One of the most potent and representative compound **64** was used as a template for superimposition, assuming that its lowest energy conformation represents a bioactive conformation at receptor active site level. The minimum energy conformer of compound **64** was obtained and the geometry optimized molecules were aligned on it by common substructure alignment using ALIGN DATABASE command in SYBYL. The determined conformation for the alignment is shown in Fig. 1. It can be seen that all the studied compounds have similar active conformations.

Molecular docking

Molecular docking is a potent method in drug discovery process that simulates conformations of small compounds in protein binding sites (Azizian *et al*., 2012). Here to locate the appropriate binding orientations and find existing interactions of pyrazolo[1,5-α] pyrimidine derivatives with MAPKAP-K2 docking study was performed with the AutoDock 4.2 program (Morris *et al*., 2009). The protein complexes were selected from protein databank (http://www.rcsb.org). Among crystallized complexes, PDB ID: 3A2C (Fujino *et al*., 2010) was selected based on the resolution and the size of the co-crystal ligand which is similar to experiment set. Initially, protein was prepared by removing all water molecules, and adds polar hydrogen atoms and Kollman charges to the protein (Singh and Kollman, 1984). The grid box size and the grid spacing were set as 60 × 60 × 60 Å and 0.375 Å, respectively. At last, all derivatives were flexibly docked into the binding site. During the docking process top ten conformations were generated for each ligand based on dock score value and interactions were analyzed for appropriate orientation with lower binding energy. Pharmacophore studies have been performed by LigandScout 3.03 program (Wolber and Langer, 2005).

3D-QSAR studies

The steric and electrostatic potential fields for CoMFA were calculated at each lattice intersection of a regularly spaced grid of 2.0 Å. The lattice was defined automatically and is extended at least 4 Å beyond Van der Waals volume of all aligned molecules in *X*, *Y* and *Z* directions. A sp3 carbon atom with a van der Waals radius of 1.52 Å and charge of +1.0 served as the probe atom to calculate steric and electrostatic fields. In order to reduce noise and improve efficiency, column filtering (minimum sigma) was set to 2.0 kcal/mol, excluding from the analysis those

Table 1 Chemical structures of MAPKAP-K2 inhibitors and their experimental and predicted activity (pIC_{50})

No.[a]		R	IC_{50} (μM)	pIC_{50} (M)	CoMFA	CoMFA-2	CoMSIA
M1	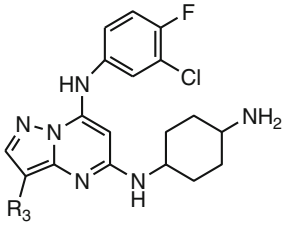	H	1.3	5.89	5.59	5.71	5.43
M22		CN	3.1	5.51	5.35	5.27	5.39
M23		Cl	8.1	5.09	5.35	5.30	5.41
M24		Br	9.2	5.04	5.29	5.22	5.40
M25	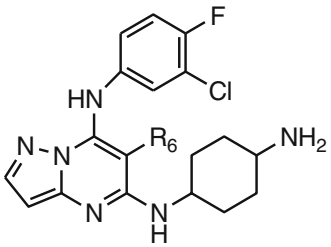	Me	0.4	6.40	6.20	6.23	5.94
M26		Et	0.4	6.40	6.19	6.24	6.19
M27		Pr	0.6	6.22	6.31	6.33	6.26
M28		Ph	1.6	5.80	5.87	5.91	6.00
M30	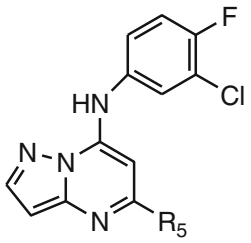	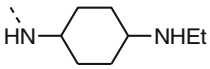	2	5.70	5.67	5.59	5.71
M34		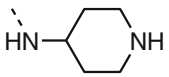	25	4.60	4.48	4.43	4.59
M35		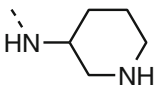	0.4	6.40	6.29	6.25	6.28
M38	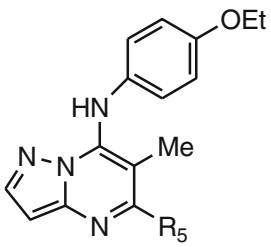	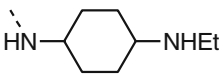	0.36	6.44	6.15	6.35	6.14
M40		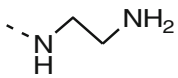	2.5	5.60	5.26	5.31	5.38
M41		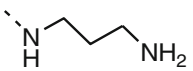	8.7	5.06	5.25	5.27	5.26

Table 1 continued

No.[a]	R	IC_{50} (μM)	pIC_{50} (M)	CoMFA	CoMFA-2	CoMSIA
M42	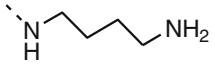	4.1	5.39	5.27	5.41	5.41
M43	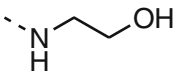	8.3	5.08	5.21	5.23	5.38
M44	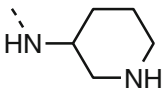	0.4	6.40	6.44	6.53	6.63
M47	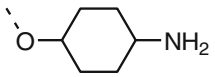	0.57	6.24	6.46	6.54	7.11
M48	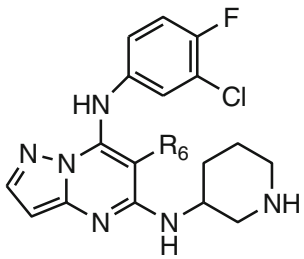 Me	0.51	6.29	6.47	6.38	6.49
M49	Et	0.7	6.15	6.53	6.41	6.42
M51	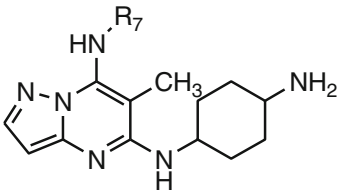 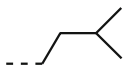	12	4.92	5.06	5.02	4.80
M52	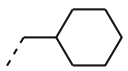	11	4.96	5.14	5.07	4.74
M53	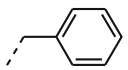	7	5.15	5.23	5.22	4.98
M54	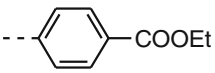	0.7	6.15	6.18	6.28	6.29
M55	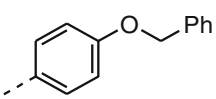	0.7	6.15	6.07	6.09	6.03

Table 1 continued

No.[a]	R	IC_{50} (μM)	pIC_{50} (M)	CoMFA	CoMFA-2	CoMSIA
M56	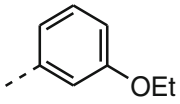	1.4	5.85	5.89	5.86	5.97
M57	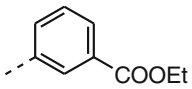	1.9	5.72	5.72	5.55	5.75
M58	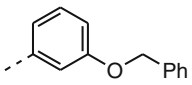	3	5.52	5.46	5.38	5.45
M59	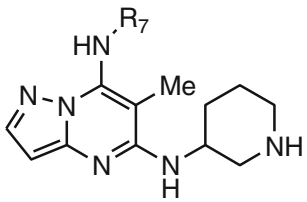 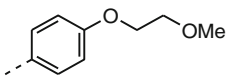	0.13	6.89	6.54	6.57	6.58
M60	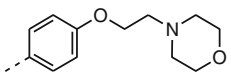	0.16	6.80	6.84	6.87	6.72
M61	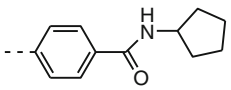	0.14	6.85	6.97	6.92	6.77
M62	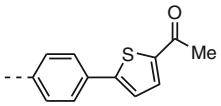	0.057	7.24	7.11	6.99	6.61
M63	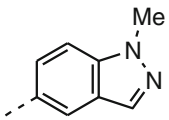	0.076	7.12	7.05	6.99	7.04
M64	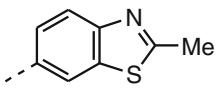	0.054	7.27	7.31	7.26	7.18
M66	Me	1.7	5.77	6.03	5.98	6.22
M67	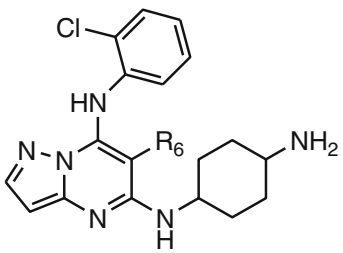 Et	1.5	5.82	6.27	6.10	6.85

[a] Numbers are according to the reference Kosugi *et al*. (2012)

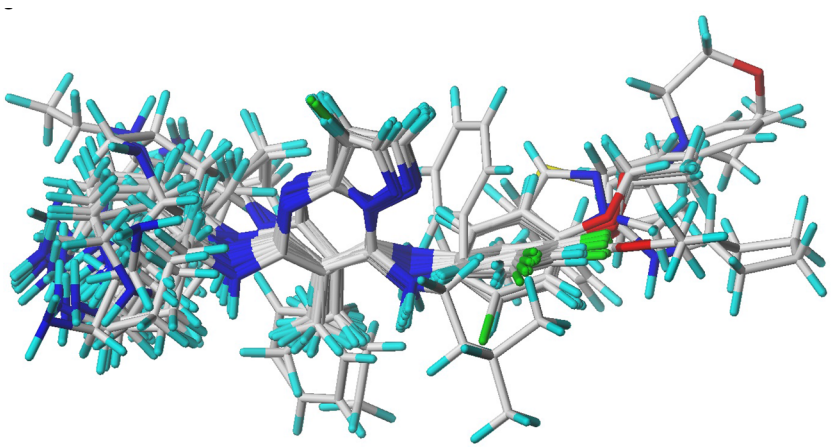

Fig. 1 Alignment of training and test set compounds on compound **64**

columns (lattice points) whose energy variance is less than this value. To reduce domination by large steric and electrostatic energies to a minimum, all energies that exceeded the cutoff value of 30 kcal/mol were passed over. CoMFA region focusing is a method of application of weights to the lattice points in a CoMFA region to enhance or attenuate the contribution of these points to subsequent analysis, here 'StDev*-Coefficients' values and different weighing factors were applied in addition to grid spacing for getting the better models.

The similarity index descriptors were calculated using the same lattice box employed for the CoMFA calculations and a sp3 carbon as probe atom with a +1 charge, +1 hydrophobicity and +1 H-bond acceptor and +1 H-bond donor properties. Steric, electrostatic, and hydrophobic as well as H-bond donor and acceptor similarity indices were calculated at each lattice intersection of a regular-spaced grid of 2.0 Å. Similarity indices were calculated between the probe, and each atom of the molecules based on a Gaussian distance function (Klebe *et al*., 1994). The steric indices are related to the third power of the atomic radii; electrostatic descriptors are derived from the atomic partial charge (Kubinyi, 1993), hydrophobic fields are derived from atom-based parameters (Viswanadhan *et al*., 1989), and hydrogen bond donor and acceptor indices are obtained by a rule-based method based on the experimental results (Kubinyi, 1993). During the cross-validation analysis, column filtering was set to 1.0 kcal/mol.

Partial Least Square (PLS) methodology was performed to quantify the relationships between the CoMFA and CoMSIA descriptors and the biological activities. The cross-validation (Cramer *et al.*, 1988; Wold, 1978) analysis was performed using the leave one out (LOO) method in which one compound is removed from the data set, and its activity is predicted using the model derived from the rest of the dataset. It results in the cross-validation correlation coefficient (q^2) and the optimum number of components *N*. The PLS analysis was performed without cross-validation, applying no column filtering. After this, the squared correlation coefficient (r^2) values, standard error of predictions (SEP) and *F* values are calculated. The boot strapping (Wehrens *et al*., 2000) and the leave-many-out cross-validation (ten groups) were carried out and confirmed by the average value for 100 runs from each cross-validation. To test the utility of the model as a predictive tool, an external set of compounds (the test set) with known activities, but not used in model generation, was used.

Results and discussion

Molecular docking studies

To get more insight into the protein inhibitor interactions and the structural features of active site of protein, docking methodology could offer valuable information. Firstly, to ensure next binding mode predictions accuracy of compounds with target protein, the co-crystallized ligand (*N*7-(4-ethoxyphenyl)-6-methyl-*N*5-[(3S)-piperidin-3-yl]pyrazolo[1,5-a]pyrimidine-5,7-diamine) (PYD) has been re-docked into the active site of MAPKAP-K2. Resulted conformation corresponds to the lowest energy score that was selected as the most probable binding conformation. Consequently, by superimposition of the redocked PDY and crystallized one, RMSD <0.4 Å has been achieved (Fig. 2) which suggests a high docking reliability of program. Therefore, the AutoDock 4.2 docking protocol and applied parameters could be used to find binding mode of other inhibitors in this research with MAPKAP-K2.

All studied inhibitors were also docked into the binding site of protein. Generally, inhibitors show hydrogen bond, hydrophobic and positive electrostatic interactions with Glu 145, Leu 141 and Ala 91, Val 78 and Asp 207, respectively, which were considered to be crucial for

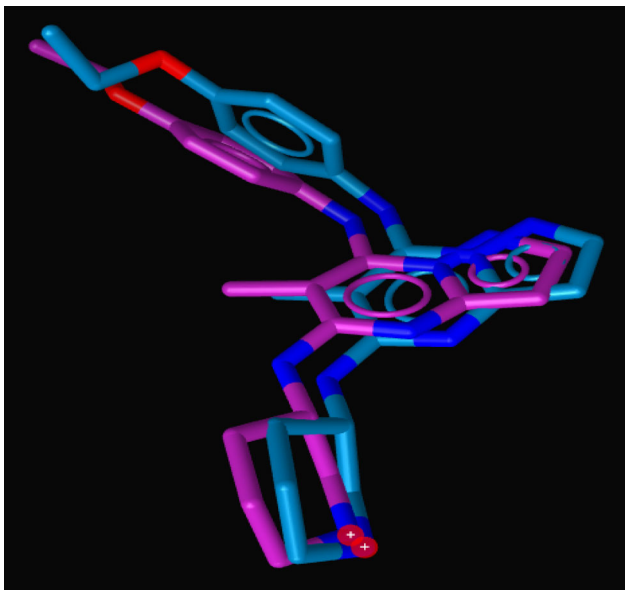

Fig. 2 Structure overlaps between co-crystal and docked orientation

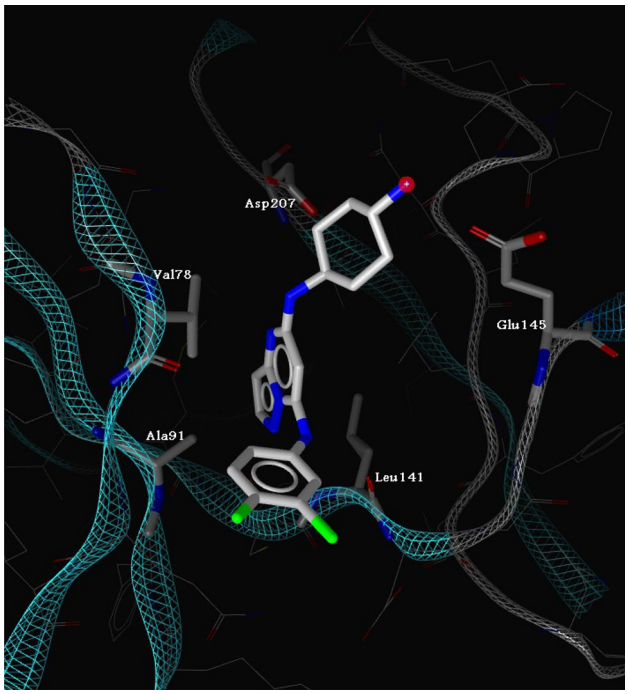

Fig. 3 Hit molecule position in the active site of enzyme and critical amino acids in its stabilization

inhibitory activity. Figure 3 represents the binding orientation of compound (**1**) and also shows how well the compound fits into active site of MAPKAP-K2. It can be concluded that meta substitute piperidine (**35**) in comparison with 4-substitute (**34**) results in better positive electrostatic interaction of nitrogen atom with residues. In this regard, appropriate distance between two nitrogen atoms in R_1 position play crucial role which is obvious in **40**–**42**. Overlay, fused structure in this part makes appropriate placement of nitrogen atom and better electrostatic interaction than other derivatives (**44** against **40**). In compounds **59**–**64**, if phenyl ring in R_1 position has higher electron density, more potent hydrophobic interaction could be formed (**63**–**64**), and the compound shows high potency through inhibition of enzyme. Indeed, from Table 1 compound **59** shows the lowest binding energy. This effect have critical rule in inhibition of compound **38** as compared to **47** within which electron donor ethyl groups induced built of electrostatic interaction in this region. On the other hand, electron acceptor groups on pyrazole part of compounds (**22**–**24**) deplete charge on N atom, and result in elimination of crucial H-bond interaction with Leu 141. Finally, presence of methyl or ethyl groups in **25** and **26**, respectively, do not make significant change in inhibition, but inserting bulkier groups such as phenyl (**28**) decrease inhibition because of steric hindrance in stabilizing of compound into the binding pocket (data not shown).

We selected the most potent inhibitor **64** in the experiment to perform the deeper docking study. Figure 4 represents the interaction model of that with MAPKAP-K2, in which inhibitor is suitably situated at the binding site and there are various interactions between it and the binding region of the enzyme. The two-dimensional representation for the interaction mode between compound and MAPKAP-K2 generated by the Ligandscout 3.03 program is shown in Fig. 5.

Three hydrogen bonds between compound 64 and active site of MAPKAP-K2 (Glu 141 and Leu 141) are formed, as

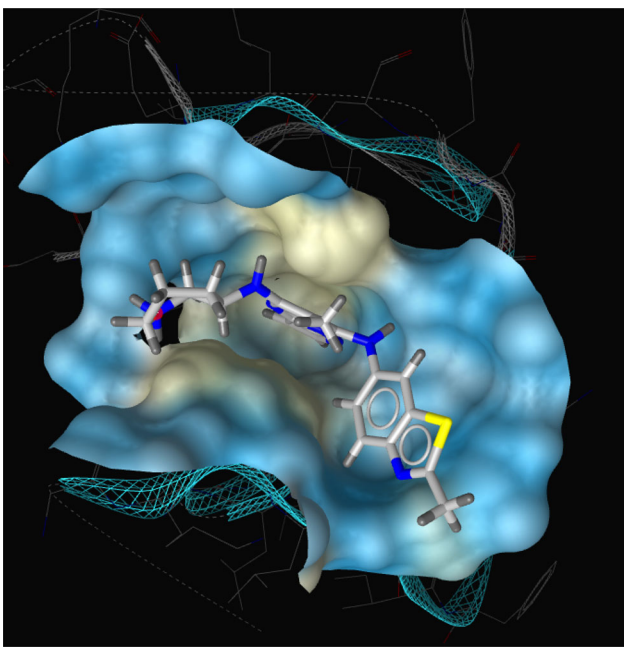

Fig. 4 Docking conformation of the most potent inhibitor 64 with corresponding binding pocket of MAPKAP-K2

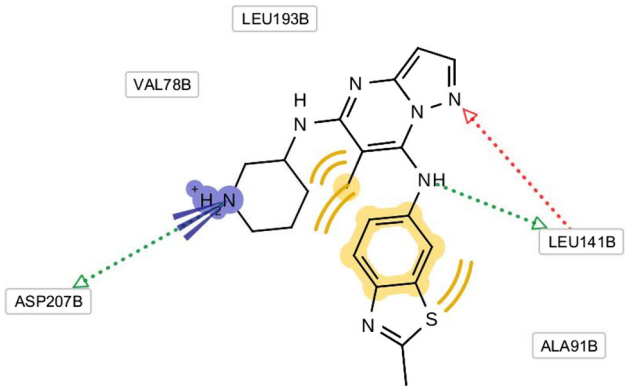

Fig. 5 2D structure of interaction sketched by LigandScout 3.03 program

well as the electrostatic interaction between the piperidine group and Asp 207. The phenyl and methyl groups also trigger hydrophobic interactions with some residues in the pocket (Ala 91 and Val 78). Therefore, according to structural analyses and study of existing interactions, it can concluded that these residues play important role in compound inhibition potency through MAPKAP-K2.

3D-QSAR studies

CoMFA analysis

The PLS method was used to construct 3D-QSAR model relating molecular descriptors with inhibitory activities. The data set was divided into a training set of 29 molecules and a test set of 7 molecules, which was drawn out one-fifth from the 36 compounds as a test set, every five compounds were selected. The best model for the alignment of compounds was selected based on the PLS statistical analysis.

In the CoMFA model, an optimum number of components of five with a q^2 of 0.502 and an SEP of 0.537 were obtained. According to the fact that q^2 coefficient is usually used as a measure of 3D-QSAR quality, the value of 0.502 indicates a reasonable correlation. The non-cross validated PLS analysis with the five optimum components revealed a conventional r^2 value of 0.942, $F = 74.833$ and an estimated standard error (SEE) of 0.183. The steric field descriptors explain 84.7 % of the variance, while the electrostatic descriptors explain 15.3 %. To support the statistical validity of these models, 100 runs of bootstrapping method were produced to determine the error on the r^2 ($r^2_{\text{bootstrap}}$) and the standard error of estimate ($S_{\text{bootstrap}}$). An average $r^2_{\text{bootstrap}}$ value of 0.948 ± 0.008 and an $S_{\text{bootstrap}}$ value of 0.100 ± 0.071 demonstrate that the CoMFA model is very stable, possesses a statistical significance and a good predictive ability. All statistical parameters supporting CoMFA-1 model are reported in Table 2.

Table 2 Statistical results of CoMFA and best CoMSIA models

	CoMFA-1	CoMFA-2 (after region focusing)	CoMSIA-3 (Best model)
PLS statistics			
LOO cross q^2/SEP	0.502/0.537	0.602/0.480	0.546/0.525
Group cross q^2/SEP	0.504/0.548	0.616/0.472	0.532/0.533
Non-validated r^2/SEE	0.942/0.183	0.955/0.161	0.891/0.257
F	74.833	98.670	29.924
$r^2_{\text{bootstrap}}$	0.984 ± 0.008	0.970 ± 0.009	0.927 ± 0.026
$S_{\text{bootstrap}}$	0.100 ± 0.071	0.123 ± 0.079	0.200 ± 0.123
Optimal compounds	5	5	6
r^2_{test}	0.852	0.874	0.507
Field distribution %			
Steric	0.847	0.825	1.00
Electrostatic	0.153	0.175	–
Hydrophobic	–	–	–
H-bond donor	–	–	–
H-bond acceptor	–	–	–

The predicted pIC_{50} values for the training set and test set compounds are given in Table 1. Figure 6a shows the relationship between the CoMFA-1 predicted and experimental pIC_{50} values of the non-cross validated analyses. From Fig. 6a, it can be seen that all points are located on the diagonal line.

Region focusing was considered as an additional strategy to improve q^2. A new model (CoMFA-2) was generated with increased predictive power (q^2), enhanced resolution, tighter grid spacing, and greater stability at the same number of components. It can be seen from the model CoMFA-2 in Table 2 that the application of region focusing resulted in a significant increase from 0.502 to 0.602 for the internal validity (q^2) and with small effect to the non-validated r^2. The steric and electrostatic field contributions to the final CoMFA-2 model were 82.5 and 17.5 %, respectively. The correlation between the predicted activities and the experimental activities by CoMFA-2 model are depicted in Fig. 6b. The high q^2, r^2, and F values, along with the low SEE value, indicated a good statistical correlation and reasonable predictability of the CoMFA-2 model.

CoMSIA analysis

The CoMSIA method defines explicit hydrophobic, hydrogen bond donor and acceptor descriptors in addition

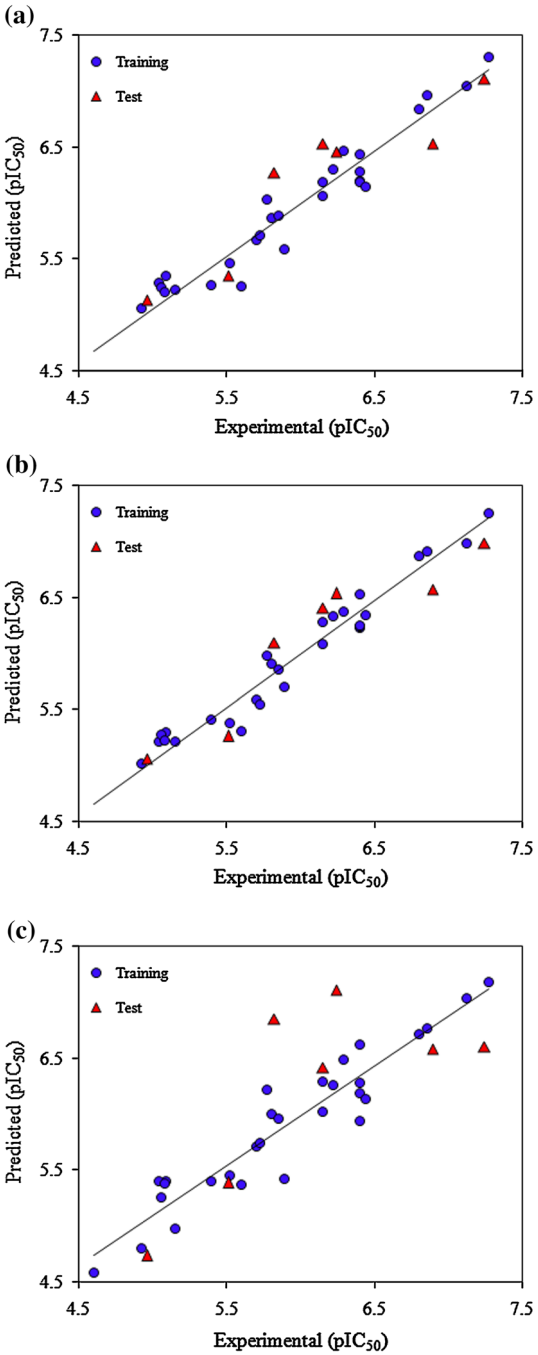

Fig. 6 Plot of experimental against predicted pIC_{50} by CoMFA (**a**), CoMFA region focusing (**b**) and CoMSIA (**c**)

to steric and electrostatic fields used in CoMFA. Former studies demonstrated that the five CoMSIA descriptors dependency may reduce the model significance and predictivity (Bringmann and Rummey, 2003; Bohm *et al.*, 1999). For this reason, all 31 possible descriptors' combinations were calculated with their respective q^2 value and optimum number of components (Fig. 7). As can be seen from Fig. 7, The steric field presents the highest q^2 value (0.546) and was then selected for further analysis. The groups cross q^2 value of 0.532, and bootstrapped r^2 value of 0.927 ± 0.026 conformed to that was the best CoMSIA model. This model was subsequently selected to generate the final CoMSIA model. We also used the CoMSIA-3 model to predict the activities of the test set compounds (Table 1). The correlation between the predicted activities and the experimental activities are presented in Fig. 6c.

Model validation and selection

All 3D-QSAR statistical results are summarized in Table 2. However, the CoMSIA model produced good results for the training set ($r^2 = 0.891$), but it did not produce good results for the test set ($r^2_{test} = 0.507$). So, the two CoMFA models are superior to the CoMSIA model. Also, from the two CoMFA models, the CoMFA-2 (after region focusing) model has the good statistical results than the CoMFA-1 model. Therefore, taking all statistical results into account, the CoMFA-2 model has been selected for the structural analysis.

Steric contour maps

The steric contour map of the CoMFA-2 model is shown in Fig. 8a. Compound **64** was used as the reference molecule. The green contours (80 % contribution) represent regions where bulky substituents would increase the activity, while the yellow contours (20 % contribution) represent regions where the steric bulky group would be unfavorable.

The steric contour map of CoMFA-2 region focusing (Fig. 8a) shows two green contours. One is near the substituent R_5, and the other is near the substituent R_6. This indicates that bulky substituents are preferred in these areas in order to produce higher MAPKAP-K2 inhibitory activity.

Several yellow regions near the R_3, R_5 and R_7 positions indicate that the less bulky substituents are preferred for higher activity. One of the large yellow regions is around R_3. This can be explained by the fact that the compounds with a small H substitution in the R_3 area, e.g., compound **1**, is highly active as compared to compounds **22**, **23** and **24**, which have large substituent (CN, Cl, Br) in this area leading to loss of activity.

Another yellow region is found around the R_5 position. This can also explain why compounds **30**, and **34** and also **40**, **41** and **42**, which have the same group at every position except the R_5 position, have very different activities. This contour map suggests that compounds with steric bulky group substituents at R_3, R_5 and R_7 positions would be beneficial for enhanced activity.

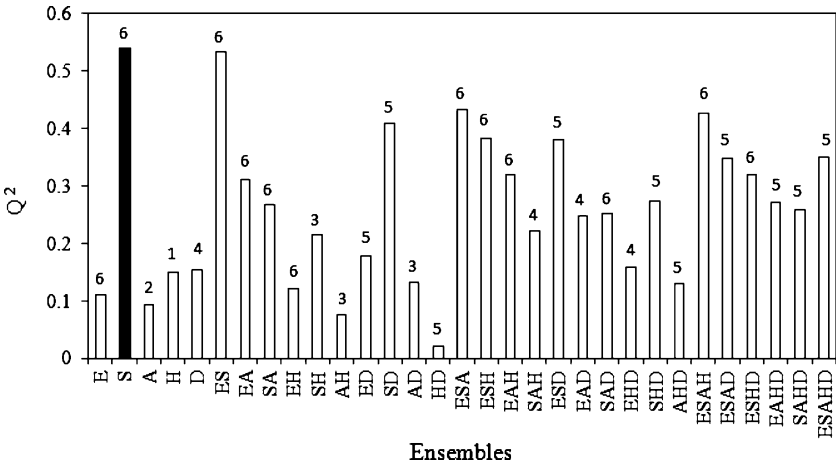

Fig. 7 Graph of the 31 possible CoMSIA descriptors combinations (*S* steric, *E* electrostatic, *H* hydrophobic, *D/A* H-bond donor/acceptor) with their respective q^2 values above the bars reporting their optimal number of components

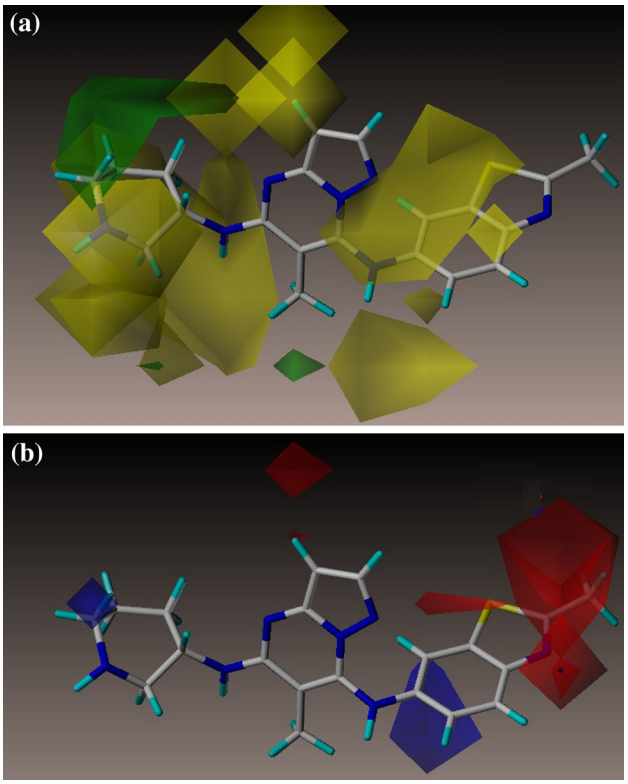

Fig. 8 Contour maps of CoMFA region focusing: steric (**a**) and electrostatic (**b**) based on compound **64**

Electrostatic contour maps

The CoMFA electrostatic contour plots are displayed in Fig. 8b for CoMFA-2 model. Two blue contour maps exist behind the benzothiazole rings (R_7) and in front of the piperidine ring (R_5), indicating that any positive charge or electron deficient substitute will enhance the activity at these positions.

According to the molecular **53**, **54**, **59** and **62** in the dataset (see Table 1), the comparison of **53** with **54** and **59** with **62** shows that both pair molecules have the same structure except in the R_7 position. While the **54** and **62** have electron withdrawing groups at the R_7 substituted than the **53** and **59** have electron donating groups at same position, respectively. Hence, the activity (pIC_{50}) of the compounds **54** and **62** are higher than the **53** and **59**, respectively.

For the electrostatic CoMFA map (Fig. 8b), the two red regions are found in front of the thiazole and near the pyrazole rings. These regions indicate that any negative charge or electron donor substitute will enhance the activity at these positions.

For example, compounds **55** and **56**, which contain higher electronegative groups of phenylmethoxy and ethoxy at the R_7 substituent, respectively, have higher activity than compound **53**. For another example, compounds **22**, **23** and **24** with the higher electron withdrawing groups at the R_3 position (near the pyrazole rings) also show lower activity than compounds **1**.

According to the detailed contour analyses of CoMFA-2 model, several useful information on the structural requirements for the observed inhibitory activities was obtained. So, the docking results, CoMFA and CoMSIA analyses can be extremely useful in the design of new chemical moieties based on a prediction of their MAPKAP-K2 inhibitory activities.

Conclusion

In present study, 3-D QSAR analysis and docking studies were performed on recently synthesized pyrazolo[1,5-α] pyrimidine derivatives. Analysis of CoMFA and CoMSIA results showed CoMFA model to be more predictive than CoMSIA model. The CoMFA region focusing model provided the most significant correlation of steric and electrostatic fields with the MAPKAP-K2 inhibitory activities.

3-D QSAR contour maps derived gave useful information about designing of new MAPKAP-K2 inhibitors. Docking study revealed that the three hydrogen bonds between most active compound (**64**) and active site of MAPKAP-K2 (Glu 141 and Leu 141) are formed, as well as the electrostatic interaction between the piperidine group and Asp 207. The phenyl and methyl groups also trigger hydrophobic interactions with some residues in the pocket (Ala 91 and Val 78). The above information can be used to design new lead compounds showing higher inhibitory activities and the chemical synthesis of new compounds is in progress.

Acknowledgments This research was supported by a grant from the Research Council of Tehran University of Medical Sciences.

References

Adams JL, Badger AM, Kumar S, Lee JC (2001) 1 p38 MAP kinase: molecular target for the inhibition of pro-inflammatory cytokines. Prog Med Chem 38:1–60

Anderson DR, Meyers MJ, Vernier WF, Mahoney MW, Kurumbail RG, Caspers N, Poda GI, Schindler JF, Reitz DB, Mourey RJ (2007) Pyrrolopyridine inhibitors of mitogen-activated protein kinase-activated protein kinase 2 (MK-2). J Med Chem 50: 2647–2654

Arend WP, Dayer JM (1990) Cytokines and cytokine inhibitors or antagonists in rheumatoid arthritis. Arthr Rheum 33:305–315

Azizian H, Nabati F, Sharifi A, Siavoshi F, Mahdavi M, Amanlou M (2012) Large-scale virtual screening for the identification of new Helicobacter pylori urease inhibitor scaffolds. J Mol Model 18: 2917–2927

Bohm M, Sturzebecher J, Klebe G (1999) Three-dimensional quantitative structure-activity relationship analyses using comparative molecular field analysis and comparative molecular similarity indices analysis to elucidate selectivity differences of inhibitors binding to trypsin, thrombin, and factor Xa. J Med Chem 42:458–477

Bringmann G, Rummey C (2003) 3D QSAR investigations on antimalarial naphthylisoquinoline alkaloids by comparative molecular similarity indices analysis (CoMSIA), based on different alignment approaches. J Chem Inf Comp Sci 43:304–316

Camussi G, Lupia E (1998) The future role of anti-tumour necrosis factor (TNF) products in the treatment of rheumatoid arthritis. Drugs 55:613–620

Clark M, Cramer RD, Vanopdenbosch N (1989) Validation of the general purpose tripos 5.2 force-field. J Comput Chem 10: 982–1012

Cobb MH, Goldsmith EJ (1995) How MAP kinases are regulated. J Biol Chem 270:14843–14846

Cramer RD, Patterson DE, Bunce JD (1988) Comparative molecular field analysis (CoMFA). 1. Effect of shape on binding of steroids to carrier proteins. J Am Chem Soc 110:5959–5967

Dayer JM, Demczuk S (1984) Cytokines and other mediators in rheumatoid arthritis. Springer Semin Immunopathol 7:387–413

Dinarello CA (1991) Inflammatory cytokines: interleukin-1 and tumor necrosis factor as effector molecules in autoimmune diseases. Curr Opin Immunol 3:941–948

Drews J (2000) Drug discovery: a historical perspective. Science 287:1960–1964

Fujino A, Fukushima K, Namiki N, Kosugi T, Takimoto-Kamimura M (2010) Structural analysis of an MK2-inhibitor complex: insight into the regulation of the secondary structure of the Gly-rich loop by TEI-I01800. Acta Crystallogr D Biol Crystallogr 66:80–87

Gasteiger J, Marsili M (1980) Iterative partial equalization of orbital electronegativity—a rapid access to atomic charges. Tetrahedron 36:3219–3228

Gille H, Sharrocks AD, Shaw PE (1992) Phosphorylation of transcription factor p62(TCF) by MAP kinase stimulates ternary complex formation at c-fos promoter. Nature 358:414–417

Goldberg DR, Choi Y, Cogan D, Corson M, DeLeon R, Gao A, Gruenbaum L, Hao MH, Joseph D, Kashem MA, Miller C, Moss N, Netherton MR, Pargellis CP, Pelletier J, Sellati R, Skow D, Torcellini C, Tseng YC, Wang J, Wasti R, Werneburg B, Wu JP, Xiong Z (2008) Pyrazinoindolone inhibitors of MAPKAP-K2. Bioorg Med Chem Lett 18:938–941

Klebe G, Abraham U, Mietzner T (1994) Molecular similarity indices in a comparative analysis (CoMSIA) of drug molecules to correlate and predict their biological activity. J Med Chem 37:4130–4146

Kosugi T, Mitchell DR, Fujino A, Imai M, Kambe M, Kobayashi S, Makino H, Matsueda Y, Oue Y, Komatsu K, Imaizumi K, Sakai Y, Sugiura S, Takenouchi O, Unoki G, Yamakoshi Y, Cunliffe V, Frearson J, Gordon R, John Harris C, Kalloo-Hosein H, Le J, Patel G, Simpson DJ, Sherborne B, Thomas PS, Suzuki N, Takimoto-Kamimura M, Kataoka KI (2012) Mitogen-activated protein kinase-activated protein kinase 2 (MAPKAP-K2) as an antiinflammatory target: discovery and in vivo activity of selective pyrazolo[1,5-a]pyrimidine inhibitors using a focused library and structure-based optimization approach. J Med Chem 55:6700–6715

Kotlyarov A, Neininger A, Schubert C, Eckert R, Birchmeier C, Volk HD, Gaestel M (1999) MAPKAP kinase 2 is essential for LPS-induced TNF-α biosynthesis. Nat Cell Biol 1:94–97

Kubinyi H (1993) 3D QSAR in drug design: theory, methods and applications. ESCOM, Leiden

Lee JC, Laydon JT, McDonnell PC, Gallagher TF, Kumar S, Green D, McNulty D, Blumenthal MJ, Heys JR, Landvatter SW, Strickler JE, McLaughlin MM, Siemens IR, Fisher SM, Livi GP, White JR, Adams JL, Young PR (1994) A protein kinase involved in the regulation of inflammatory cytokine biosynthesis. Nature 372:739–746

Morris GM, Huey R, Lindstrom W, Sanner MF, Belew RK, Goodsell DS, Olson AJ (2009) AutoDock4 and AutoDockTools4: automated docking with selective receptor flexibility. J Comput Chem 16:2785–2791

Schlapbach A, Huppertz C (2009) Low-molecular-weight MK2 inhibitors: a tough nut to crack! Future Med Chem 1:1243–1257

Singh UC, Kollman PA (1984) An approach to computing electrostatic charges for molecules. J Comput Chem 5:129–145

Trujillo JI, Meyers MJ, Anderson DR, Hegde S, Mahoney MW, Vernier WF, Buchler IP, Wu KK, Yang S, Hartmann SJ, Reitz DB (2007) Novel tetrahydro-β-carboline-1-carboxylic acids as inhibitors of mitogen activated protein kinase-activated protein kinase 2 (MK-2). Bioorg Med Chem Lett 17:4657–4663

Viswanadhan VN, Ghose AK, Revankar GR, Robins RK (1989) Atomic physicochemical parameters for three-dimensional structure directed quantitative structure-activity relationships. 4. Additional parameters for hydrophobic and dispersive interactions and their application for an automated superposition of certain naturally occurring nucleoside antibiotics. J Chem Inf Comput Sci 29:163–172

Wehrens R, Putter H, Buydens LMC (2000) The bootstrap: a tutorial. Chemometer Intell Lab 54:35–52

Winzen R, Kracht M, Ritter B, Wilhelm A, Chen CY, Shyu AB, Müller M, Gaestel M, Resch K, Holtmann H (1999) The p38 MAP kinase pathway signals for cytokine-induced mRNA

stabilization via MAP kinase-activated protein kinase 2 and an AU-rich region-targeted mechanism. EMBO J 18:4969–4980

Wolber G, Langer T (2005) LigandScout: 3-D pharmacophores derived from protein-bound ligands and their use as virtual screening filters. J Chem Inf Model 45:160–169

Wold S (1978) Cross-validatory estimation of the number of components in factor and principal components models. Technometrics 20:397–405

Xiong Z, Gao DA, Cogan DA, Goldberg DR, Hao MH, Moss N, Pack E, Pargellis C, Skow D, Trieselmann T, Werneburg B, White A (2008) Synthesis and SAR studies of indole-based MK2 inhibitors. Bioorg Med Chem Lett 18:1994–1999